HOT PLUME TESTING FACILITY COLOGNE (HPTF): DEMONSTRATION, QUALIFICATION AND EXPLORATION TESTS WITH THE WATER-COOLED PENNSTATE-LIKE BURNER HOC2

GLASGOW, SCOTLAND | 20 – 23 MAY 2024

Dominik Saile, Daniel Kirchheck, Viktor Kühl, Ali Gülhan
DLR - German Aerospace Center, Supersonic and Hypersonic Technologies Department, Cologne, Germany, Dominik.Saile@dlr.de

KEYWORDS: wind tunnel experiments, space transportation, hot gas generator, hydrogen/oxygen combustion chamber

ABSTRACT:

The blow-down-type wind tunnel 'Vertical Test Section Cologne' (VMK) [27] of the 'German Aerospace Center' (DLR) in Cologne is used for aerothermodynamic testing of spacecraft and missiles, as well as for the flight qualification of components up to Mach 3.2. In 2017, the wind tunnel was upgraded by integrating a hydrogen and oxygen supply facility forming the newly developed 'Hot Plume Testing Facility' (HPTF) primarily for the generation of hot combustion gases in the wind tunnel environment. Hot combustion gases are a requirement for flight duplication for applications such as space transportation systems, ram- and SCRamJets. For the demonstration, qualification and exploration of the facility, tests with a capacitively cooled combustion chamber have been executed for an operating range accessible to that design. To extend the operating range, the design of the existing combustion chamber was modified to accommodate water-cooling. This combustion chamber named HOC2 was used for testing for extended testing times ($t > 40$ s) at combustion chamber pressure levels above 6.0 MPa close to stoichiometric mixture ratios. Apart from the characterization of the facility, the experiments provide insights into the development of wind tunnel model integrated combustion chambers. Research questions regarding the injector geometry, combustion chamber stability, and cooling requirements are addressed. These results are used to outline the currently-explored operational range of the HPTF. Further, the results expand the knowledge on the design of wind tunnel models with integrated combustion chambers to duplicate conditions of space transportation systems in flight. This capability to conduct wind tunnel tests with realistic mixture ratios close to stoichiometric conditions is not yet existent in Europe to that scale.

1. INTRODUCTION

Space transportation systems are exposed to high mechanical and thermal loads. These loads are very challenging and base flow issues are just one of the challenging tasks that these systems are required to handle. In the past, the effect of them led to catastrophic events, such as for the failure flight (flight 157) of Ariane 5 in 2002. As the most probable reason for the failure, the inquiry board found degraded thermal condition of the nozzle of the Vulcain 2 engine due to fissures in the cooling tubes. The board concluded that loads to which the Vulcain 2 engine is subjected during flight were not exhaustively defined [20]. Needless to say, that it is crucial to correctly predict and specify the mechanical and thermal loads on space transportation systems in the future.

One of the means to address these issues are appropriate testing facilities, the capabilities of which were identified European Space Agency (ESA) as incomplete. Consequently, ESA funded in 2011 a study on 'Hot Testing Facilities for ELV Propulsion Characterization'. This was the starting point for the development of the 'Hot Plume Testing Facility' HPTF at the 'Supersonic and Hypersonic Technologies Department' at the 'German Aerospace Center' (DLR) resulting in a prove of concept [22] and design considerations for the wind tunnel [23] and the combustion chamber [24]. In 2017, the HPTF was completed. The progression of which is documented in [7-9]. The HPTF consists of the blow-down type wind tunnel 'Vertical Test Section Cologne' (VMK) and the newly-developed, integrated hydrogen and oxygen supply facility. The HPTF is primarily used for the supply of combustion gases to a combustion chamber in a wind tunnel model, where hot exhaust gases are generated and expelled through a nozzle. Hot combustion gases are a requirement for flight duplication for applications such as space transportation systems, ram- and SCRam-jets.

Subsequently, the HPTF has been used for testing in several German and international projects such as for the plume interaction activity Transregio 40 (TRR40) [12,13] or for RETALT [17] and RETPRO [11] where retropropulsion effects were investigated. Apart from wind tunnel tests with

integrated combustion chambers, the individual supply lines can also be used for tests with only either one of the two species. In other words, the oxygen supply line can be used to test hybrid rocket combustion chambers. Vice versa, hydrogen can be injected into the combustion chamber of ram or SCRam jets for testing.
In the years after the completion of the facility, various campaigns were executed to characterize the operational range of the HPTF [10,14]. For the characterization the combustion chamber 'Hydrogen Oxygen Combustor 1' (HOC1), that closely resembles the PennState burner [16, 18, 26], was developed, built and operated. As it can be seen in [10] and [14], the operational range of the facility for mixture ratios 0.7 < OFR < 3.0 was successfully tested and validated. The tests were limited to that range and to relatively short run times between 10 and 40 seconds due to the design concept of the combustion chamber, which is based on capacitive cooling.
To access the potential of the HPTF, the existing combustion chamber HOC1 had to be modified to facilitate water cooling. This system is referred to as HOC2. As shown in the paper at hand, HOC2 was used for testing over an extended period of time (t > 40 seconds) at combustion chamber pressure levels above 6.0 MPa close to stochiometric mixture ratios. Apart from the demonstration, qualification and exploration of the facility, the results provide insights into the development of wind tunnel model integrated combustion chambers.
In summary, the objective of the paper at hand is twofold: explore and extend the operational range of HPTF, while simultaneously investigate the characteristics of HOC2. Consequently, the paper tackles the following tasks:

- Demonstrate and qualify high mixture ratio, high pressure tests with gaseous oxygen and hydrogen in the HPTF with HOC2.
- Explore and extend operational range of HPTF and HOC2. Outline the currently-explored operational range.
- Assess HOC2 combustion aspects such as combustion roughness as a function of the injector geometry, mixture ratio, and nozzle throat.
- Assess water-cooling approach for HOC2.

The results expand the knowledge on the design of wind tunnel models with integrated combustion chambers to duplicate conditions of space transportation systems in flight. This capability to conduct wind tunnel tests with hot exhaust plumes generated with realistic mixture ratios close to stoichiometric conditions is not yet existent in Europe to that scale.

2. METHODS

The HPTF consists of the and oxygen supply facility integrated in VMK. The latter, VMK [27], is a blow-down type wind tunnel of the DLR Supersonic and Hypersonic Technologies Department in Cologne equipped with an open vertical free stream test section. It is used for aerothermodynamic testing of spacecraft and missiles, as well as for the flight qualification of components from the subsonic range up to Mach 3.2 at maximum reservoir conditions of 3.5 MPa and 750 K (see VMK). The fuel gas supply facility is able to provide oxygen and hydrogen at a mass flow rate of m_{O2} = 397.4 g/s and m_{H2} = 66.4 g/s, respectively, up to a maximum pressure of 11.5 MPa [10].
In the past, the PennState-like burner [16, 18] HOC1 was used as test specimen [10]. HOC1 is equipped with a single element GH2/GO2 shear coaxial injector and the main body is made of oxygen-free high-conductivity copper (OFHC). OFHC is advantageous due to high-conductivity property with respect to the thermal management of the combustion chamber, which is based on capacitive cooling. The thermal expansion issue is mitigated by applying disk springs that allow growth of the chamber in the axial direction, while simultaneously maintaining the axial force to keep the various modules in place. The combustor is rated for a maximum pressure of 7.0 MPa.
The variant used here is called HOC2. As HOC1, it is rated for a pressure level of 7.0 MPa. It features a modular design consisting of 3 OFHC blocks stacked on top of each other. Each block has a height of 75 mm and an outer diameter of 150 mm. The overall inner length of the combustion chamber (injector face plate to the nozzle throat) is 257 mm, while the inner diameter is 38 mm. Ignition is initialized with a spark plug.
To withstand higher-mixture ratios for continuous operation (in comparison to HOC1), HOC2 was equipped with 18 cooling channels with a diameter of 7.0 mm arranged in circle with a diameter of 60 mm around the inner wall. Fig. 1 shows a picture of HOC2 as integrated in VMK where the blue tubes attached to the bottom show how cooling water is transferred to the cooling channels and returned. The sketch of HOC2 in Fig. 2 with a cut-away visualizes the cooling channels where the channels marked in red and yellow represent the 9 feed and 9 return channels.
The design for the cooling of the throat is depicted Fig. 3. Water is pumped into the throat area, detours first radially, then circumstantially before being deflected in the axial return channel. The same principle was applied to realize various throat diameters. The throat diameter used for the experiments here is either D_{th} = 8.0 mm or 8.2 mm.
To drive the cooling water through the channels, a pressurized vessel was installed upstream of the cooling water supply chain. With a pressure regulator, the pressure in the vessel was set to 4.0 bar. For the configuration at hand, this led to a constant cool water supply of about 75 l/min or 1.25 kg/s.

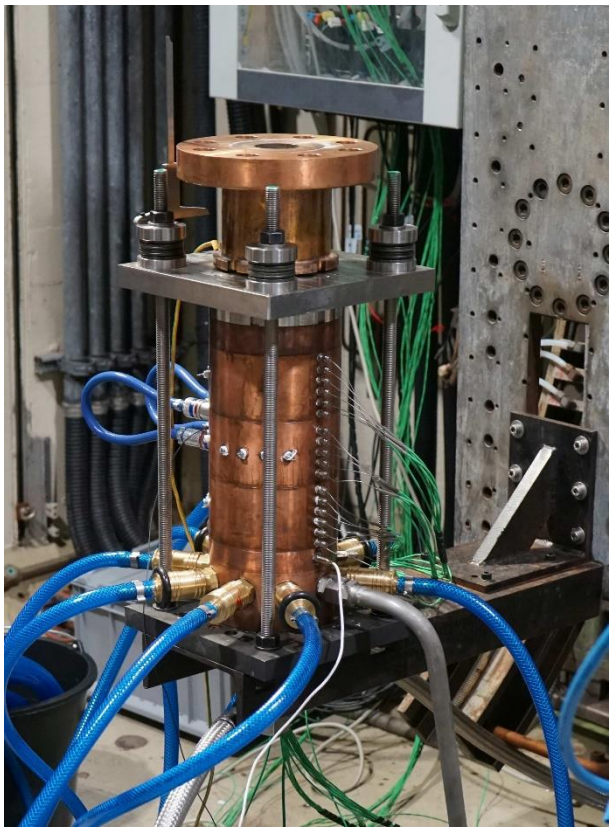

Figure 1. Picture of the combustion chamber HOC2 installed in the wind tunnel VMK

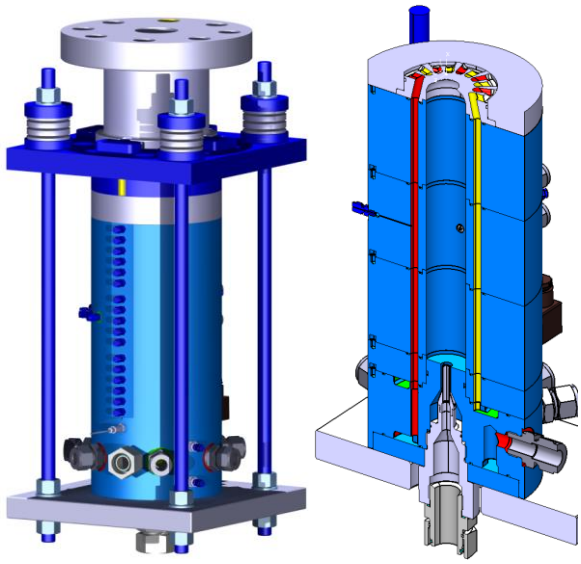

Figure 2. CAD illustration and schematic sketch of cross-sectional view of HOC2 showing the cooling channels

Note that due to the cooling channels and the abandonment of the capacitive cooling concept, the outer diameter of HOC2 could be significantly be reduced. This was not pursued here since that design modification from HOC1 to HOC2 was the fastest way forward in an ongoing project where cooling was required. Improved versions are under development. Since the injector geometry can have a significant influence on the combustion stability, four injector geometries were manufactured and tested. A sketch of the injector design is provided

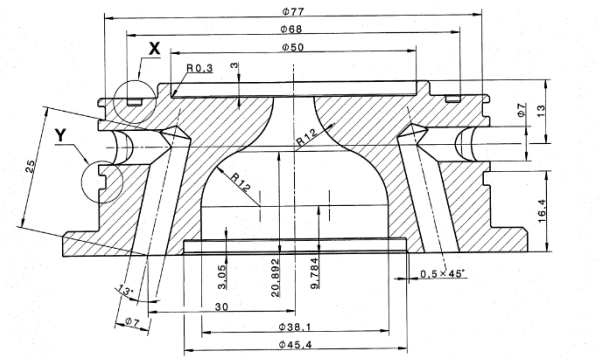

Figure 3. Cross-sectional view of the water-cooled nozzle

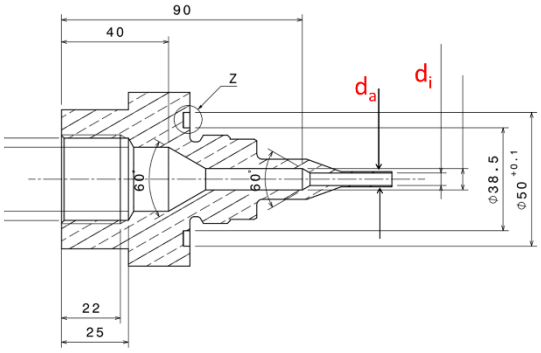

Figure 4. Cross-sectional view of the Injector element for HOC2

in Fig. 4, while the integration method can be extracted from Fig. 2. The main varied parameters are the inner and annulus diameter of the injector marked as d_i and d_a, respectively. The corresponding values are given in the in Tab. 1 for the four injectors named I-0, I-1, I-2, and I-3. The diameter at the face plate and the recess from that remain the same for all configurations, meaning D = 9.4 mm and r = 1.3 mm, respectively.

Table 1. Geometry of the shear coaxial injector

Inj.	d_i	d_a	t	D	β	A_r
	mm	mm	mm	mm	–	–
I-0	4.6	5.7	0.55	9.4	2.04	2.64
I-1	5.6	6.5	0.45	9.4	1.68	1.47
I-2	6.1	7.25	0.575	9.4	1.54	0.96
I-3	6.75	7.85	0.55	9.4	1.39	0.59

Additionally, the diameter ratio β = Do/Di and the aspect ratio $A_r = A_o/A_i$ are provided. As before, the injector design is derived from the coaxial, single-element PennState injector [18].

To measure the conditions of the chamber, the combustor is equipped with pressure transducers and 23 thermocouples. The first is used to measure the combustion chamber pressure. In detail, the pressure is measured at the face plate of the injector with the pressure transducer XTEH-7L-190SM by Kulite (combined non-linearity, hysteresis and repeatability: ±0.1 % FSO BFSL (Typ.)). The latter refer to the Type K class 1 thermocouples (diameter 1.0 mm), which are flush-mounted in open tabs

along the inner surface of the chamber in the axial and radial direction. The objective of the temperature measurements is to gain insights into the temperature distribution. Two of the thermocouples are used to measure the inflow and outflow temperature of the cooling water. The mass flow of the cooling water is captured with the ultrasonic flow meter ifm-SU9000 by ifm (accuracy: < ±3 % measured value + 0.2 % final value of the measuring range).

The inflow conditions on the gas supply chain are measured with the permanently installed sensors of the HPTF. The sensor data relevant for the case at hand are the mass flow measurements of the combustion gases and the pressure just upstream from the combustion chamber in the supply chains. The first is measured with CNGmass DCI coriolis flowmeters (max. measurement error mass flow: ±0.5 % of batch), the latter with the absolute pressure gauges CERABAR-S PMP 71 (accuracy: 0.05 %). Both measurement devices are from Endress+Hauser.

The HPTF facility has access to the data acquisition used for wind tunnel testing in VMK. It consists of a system by National Instruments equipped with the voltage input module SCXI-1102 and the train/bridge input module SCXI-1520 for capturing the data for thermocouples and pressure sensors, respectively, which are A/D converted by means of the PXI multifunction I/O module PXI-6289. The various modules are contained in the chassis PXI-1050. For the case at hand, data was acquired at 2 kHz.

For the exploration of operational range of the HPTF, a measurement matrix was defined that outlined a rectangular field in the corresponding diagram ranging from a mixture ratio OFR = 1.7 and to a pressure level of p_{CC} = 3.2 MPa to 6.6 and p_{CC} = 6.5 MPa, respectively. In detail, tests were executed with the combinations of mixture ratios at 1.7, 3.3, 5.0, 6.6 and combustion pressure levels in the range of $p_{CC,max}$ = 3.4, 4.0, 4.8, 5.9, 6.3 MPa. To reach these pressure levels, the conditions in HPTF were set to the following nominal pressure levels: $p_{CC,nom}$ = 4.0, 5.0, 6.0, 7.0, 8.0 MPa. The most challenging test with respect to heat loads took place with a mixture ratio of OFR = 6.6 at 6.2 MPa. An overview of the measurement matrix is provided in Tab. 2.

This table also outlines the basic structure of the article. 'R' indicates the reference condition that is used in most plots for comparisons. Comparisons are made between various injectors either with respect to pressure fluctuations to the heat flux. The corresponding experiments labelled as 'I-F' or as 'I-H', respectively. The experiments used to compare the influence of the mixture ratio are labelled with an 'O'. The letter 'L' and 'H' mark the experiments used as example for long runs or to identify high heat flux run.

3. RESULTS

3.1. Operational range of HPTF

One of the main drivers for the tests was the demonstration, qualification and exploration of the HPTF and to extend the so-far established operational range. This was done by carefully increasing the challenge for the newly-developed combustion chamber, meaning by adjusting the conditions to higher mixture ratios, higher combustion chamber pressures and longer run times. All tests outlined in the measurement matrix above were successful (details to the combustion chamber's response are provided in Ch. 3.2). Thus, the input conditions of which were used to outline the extended operational range, which is shown in Fig. 5. While the range marked in red shows the previously examined operational range, the newly-established range with tests using HOC2 is shown in green. Note that each grey circle represents an executed experiment. The results validate the capability of both, combustion chamber HOC2 and HPT-facility, for 'long' tests up pressure levels in the range of 6.0 to 7.0 MPa at a mixture ratio close to OFR ~ 7.0.

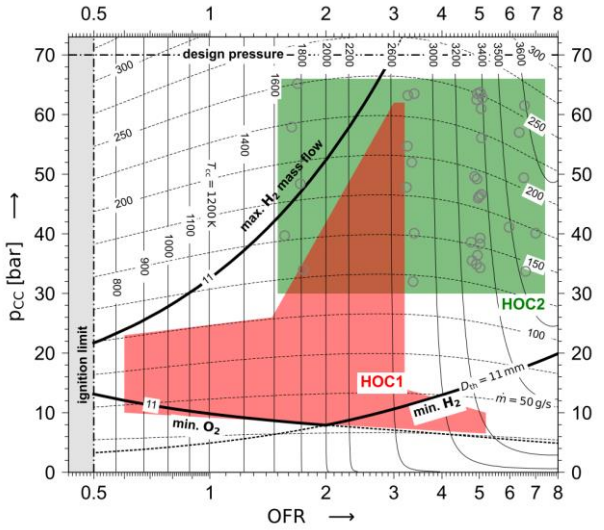

Figure 5. Explored operating range of the HPTF. The region marked in red was explored with HOC1, the region in green depicts the operational range added with the current test results with HOC2.

Note that the graph marks limitation of the operational range due to the highest possible mass flow. This is based on a throat diameter of 11 mm. It can be exceeded here since a throat diameter of ≤ 8.2 mm was used. Further, with dedicated measurement campaigns and deliberately-designed combustion chambers, the operational range can be pushed to comprise even oxidizer-rich or high-pressure regions up to 11.5 MPa. In other words, the operational range here reflects the currently explored area. The HPTF is capable to reach even more challenging conditions. Remember that the facility is rated for a maximum mass flow rate m_{O2} = 397.4 g/s and m_{H2} = 66.4 g/s for oxygen and hydrogen, respectively.

Table 1. Geometry of the shear coaxial injector

This table provides an overview of the experiments executed in HPTF with HOC2. The parameter space is described with the mixture ration OFR, the throat diameter D_{th}, the nominal combustion chamber pressure $p_{CC,nom}$, and the injector geometry (I-0 to I-4). Executed experiments are marked in green, the reference experiment is labelled with an 'R'. The labels 'L', 'O', 'I-F', and 'I-H' indicate long runs, experiments used to assess the influence of the mixture ratio, experiments to assess the influence of the injector for pressure fluctuations ('-F') or with respect to the heat flux ('-H'), respectively.

Mixture ratio	**OFR**	**1.7**		**3.3**		**5.0**		**6.6**	
Throat diameter	D_t **[mm]**	8.0	8.2	8.0	8.2	8.0	8.2	8.0	8.2
Comb. cham. pressure	**Injector**								
$p_{CC,max}$ / $p_{CC,nom}$ **[MPa]**	**No.**								
3.4 / 4.0	I-0								
	I-1								
	I-2								
	I-3								
4.0 / 5.0	I-0								
	I-1								
	I-2								
	I-3								
4.8 / 6.0	I-0						I-F		
	I-1						I-F		
	I-2						I-F		
	I-3						I-F		
5.9 / 7.0	I-0								
	I-1								
	I-2								
	I-3								
6.3 / 8.0	I-0			O/L		O/L	R	O/H	
	I-1						I-H		
	I-2						I-H		
	I-3						I-H		

3.2. Combustion chamber pressure

The pressure and pressure fluctuation evolution of two of the most challenging experiments are given in Fig. 6 and Fig. 7. Most challenging here refers to either (1) a high-pressure, close to stoichiometric mixture ratio condition or to (2) a 'long' run (see 'H' and 'L' in Tab. 2).

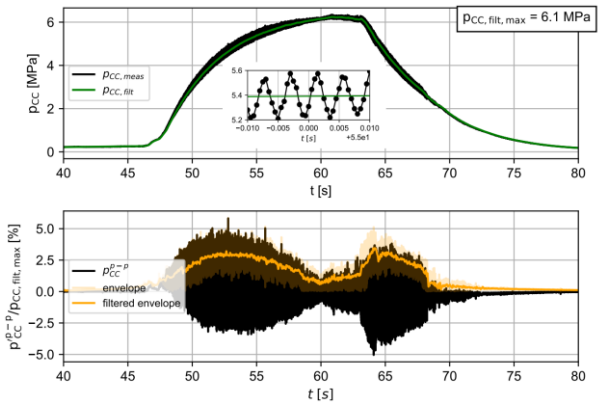

Figure 6. Pressure and pressure fluctuation evolution for a mixture ratio of OFR = 6.5 for the experiments in the 6.3 MPa-range (throat diameter D_{th} = 8.0 mm, injector I-0)

For both, the pressure evolution as measured is depicted in the top graph as black line, while the green line represents a low-pass (cut-off frequency 10 Hz) filtered data set to visualize the overall evolution. The high frequency content is visualized in the bottom graph in black as pressure fluctuation normalized with highest (low-pass filtered) combustion chamber pressure reached in that run. Additionally, the bottom graph gives an envelope (via Hilbert transform) of the normalized pressure fluctuations (orange shading) and a filtered envelope (cut-off frequency 10 Hz) (orange line) that clearly capture a quantity for the amplitude of the fluctuations. It essentially represents the temporal evolution of half the normalized peak-to-peak pressure amplitudes p'^{p-p}_{CC} /$p_{CC,filt,max}$. Note that [5] defined p'^{p-p}_{CC} /$p_{CC,filt}$ ≤ ±5% as smooth.

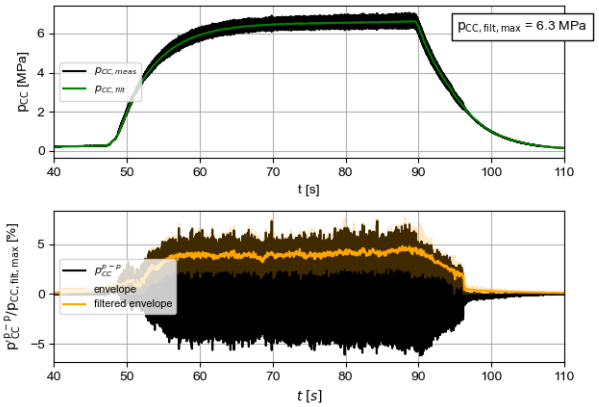

Figure 7. Pressure and pressure fluctuation evolution for a mixture ratio of OFR = 3.4 for the experiments in the 6.3 MPa-range (throat diameter D_{th} = 8.0 mm, injector I-0)

The high-pressure, high mixture ratio configuration depicted in Fig. 6 is the result of a mixture ratio of OFR = 6.5 at a mass flow rate of m_{H2} = 20.5 g/s and m_{O2} = 134.0 g/s for hydrogen and oxygen. Nominally, this would lead to a chamber pressure of 7.0 MPa, yet only $p_{CC,filt,max}$ = 6.1 MPa (87 %) is reached at the end of the run. This is predominantly attributed to the capacitive, thus transient cooling of the combustion chamber walls shifting the thermochemical equilibrium. This statement is supported by the observation that the increase follows a gradual slope before converging towards a plateau. Meanwhile, the mass flows for the supply of the combustion gases (not shown here) resemble - relatively seen - a step function reaching the nominal flow rate at t ~ 49 s. Another factor that contributes to a lower than nominal chamber pressure is the combustion efficiency, which cannot be assumed to have reached 100 %.

When it comes to the pressure fluctuations $p'_{p-p,CC}$ in the chamber (bottom graph), it can be seen that they increase at first to about ±3 % (filtered) with increasing chamber pressure where they peak before decreasing again despite the still increasing chamber pressure. It is noticeable that trend repeats for the ramp down process with a peak in a similar chamber pressure range. The cut-out in the top graph provides further insights into the frequency of the oscillations as it is sufficiently-well resolved (~ 9 data points per cycle). Under the presumption that no aliasing effect is present, the fluctuation can predominantly be attributed to a low frequency oscillation at 229 Hz. The results for the long run for a mixture ratio of OFR = 3.4 are depicted in Fig. 7. The objective of the graph here is to show that a high-pressure level (6.3 MPa) was maintained over an extended period of time ~ 30 s. The overall results for the conditions here are comparable to the previous ones, meaning 90 % of the theoretical chamber pressure is reached and the fluctuations are on the level of ±3 to ±4 % taking place with 222 Hz (at t = 69.7 s). Another long run test was executed for a higher mixture ratio of OFR = 4.9 and a shorter operating time, i.e. more than 20 s in the 6.3 MPa-range.

The results are not shown here since the previous results already proves the point to be made: The combination of HPTF and HOC2 facilitates the generation of 'smooth' high-pressure combustion gas (< ±5 %) close to stoichiometric mixture ratios that can be applied in 'long' run tests in the wind tunnel environment.

3.3. Combustion chamber pressure oscillations

Nevertheless, pressure oscillations are clearly notable in the runs before and it begs the question of their cause. Principle types of combustion instabilities [25] found in combustion chambers can be categorized with respect to their frequency range. Low frequency, intermediate frequency and high frequency instabilities are typically associated with a periodicity of (1) 10 to 400 Hz, (2) 400 to 1000 Hz, and (3) above 1000 Hz, respectively. Depending on the driving mechanism, these instabilities are called (1) chugging or feed system instabilities, (2) acoustic, buzzing or entropy waves, and (3) screaming, screeching or squealing.

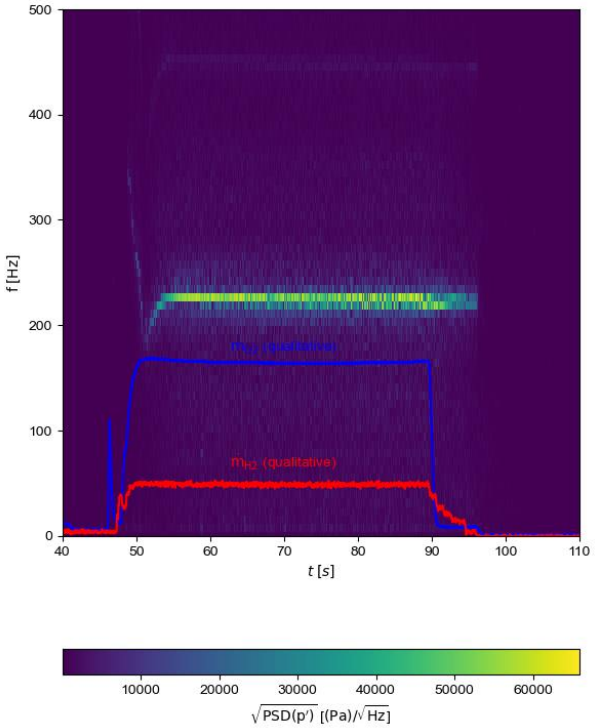

Figure 8. Spectrogram for a mixture ratio of OFR = 3.4 for the experiments in the 6.3 MPa-range (throat diameter D_{th} = 8.0 mm, injector I-0)

For further insights, a spectrogram for the long run described before (OFR = 3.4, 6.3 MPa shown in Fig. 7) is provided in Fig. 8. It shows that over the course of the gas supply ramp up, the most dominant frequency initially drops and then locks in a specific frequency between 220 to 230 Hz, where it remains constant even though the chamber pressure is still increasing and beyond the ramp down. In other words, the frequency does not show a dependency on the combustion chamber pressure, but the pressure amplitude does.

Tab. 3 and Tab. 4 list the dominant frequencies for all experiments. The frequencies of the first table are limited to injector I-O, while addressing the influence of mixture ratio the throat diameter, and the combustion chamber pressure. The second table shows the dominant frequencies for a fixed mixture ratio and throat diameter for the injectors in use, I-0 to I-3, for various chamber pressure levels. For all experiments, the most dominant frequency is locked at either 200 Hz for a mixture ratio of OFR = 1.7 or 230 Hz (±8 Hz) for the higher mixture ratios OFR = 3.3, 5.0, and 6.6 (Tab. 3). Further, a sensitivity to the injector can be noticed (Tab. 4). While the oscillations are clear and distinct (with a narrow peak) for I-0, the oscillations become more random and lose it distinctness for the other injectors: The fluctuations are found to be weakly

developed in amplitude over a larger frequency range centring at between 150 and 300 Hz, or no dominant frequency was detected.

Table 3. Dominant frequencies for injector I-0. The frequencies are provided in the unit Hertz [Hz] with an uncertainty of ±8 Hz.

Mix. ratio	**OFR**	**1.7**	**3.3**		**5.0**		**6.6**
Thr. diam.	D_t **[mm]**	8.0	8.2	8.2	8.0	8.2	8.0
Ch. press.	**Inj.**						
$p_{CC,nom}$ **[MPa]**	**No.**						
4.0	I-0	200		239		226	226
5.0		200		239		230	226
6.0		200	226	239	230	230	230
7.0		200		234		230	230
8.0		200	226	234	230	230	230

Table 4. Dominant frequencies as function of the injectors. The frequencies are provided in the unit Hertz [Hz] with an uncertainty of ±8 Hz. The label (W) indicates that only weak or not strongly developed frequencies were detected, while (NDFD) signifies that no dominant frequency was detected.

Mix. ratio	**OFR**	**5.0**			
Thr. diam.	D_t **[mm]**	8.0			
Ch. press.	**Inj. No.**	I-0	I-1	I-2	I-3
$p_{CC,nom}$ **[MPa]**					
4.0		226	200-260	150-260	150-300
5.0		230	200-260	150-260	150-300
6.0		230	200-260	150-260	150-300
7.0		230			
8.0		230	(NDFD)	150-260	(NDFD)

As shown, the predominant periodicity is in the low frequency range. No oscillations were detected in the mid or high frequency range. In literature, many cases in the low frequency range are associated with the Helmholtz resonance [3]. The fundamental concept revolves around the oscillation of the gas mass within the resonator's neck, functioning much like a mass attached to a spring. When external influences like a flow field is disrupting this mass of gas, it sets off oscillations, leading to resonance within the cavity's gas. Helmholtz oscillations are characterized by in-phase oscillating and equally distributed pressure amplitudes along the surface of the wall. Further, they are usually described as independent of the flow field and flow velocity, but [1] showed that a dependency to the mass flow rate exists. For the following first order approach, this dependency will be neglected and the Helmholtz frequencies will be calculated by $f = c/(2\pi)\ \sqrt{A/(V\ L + 2\Delta L)}$. In this case, the frequency depends on the volume of the chamber V, the cross section of the smallest cross-sectional area A, a correction factor ΔL to reflect specific design elements [2], and the speed of sound c. The correction factor is set to $\Delta L = \pi/4R$, where R corresponds to the radius of the smallest cross-section. Transferred
to the case at hand, the Helmholtz frequency can be calculated for the inlet and for the outlet, referring to the injector and the nozzle, respectively.
Due to the specifics of the setup and geometry, it is not straight forward to apply the formula to the nozzle. However, a first estimate reveal frequencies beyond 1000 Hz. For the annulus of the injector, frequencies in the range of 400 to 800 Hz are found for injector I-3 and I-0, respectively. Closest to the measured frequencies are the Helmholtz oscillations for the central part of the injector. For the case at hand, the mixture ratio of OFR = 1.7, 3.3, 5.0, and 6.6 (p_{CC} = 6.0 MPa) return speeds of sound of c = 1872 m/s, 1798 m/s, 1661 m/s, 1547 m/s [19], respectively, and this term specified by the injector geometry $\sqrt{A/(V\ L + 2\Delta L)}$ is equivalent to 0.92, 1.12, 1.21, 1.33 for injector I-0 to I-3, respectively, indicating a Helmholtz frequency range between ~227 Hz (I-0, OFR = 6.6) and 396 Hz (I-3, OFR = 1.7). Thus, it seems plausible that the Helmholtz oscillation of the central part of the injector can be attributed as governing mechanism. This statement is supported by the finding that the same frequency can be found in the supply line for oxygen, which is supplied through the central part, but not for hydrogen.
Further, since the frequencies of the annulus and the central part of the central part of the injector are relatively close, it should be kept in mind that they can resonate. A final verification of the hypothesis regarding the driving mechanism requires an in-depth analysis to exclude other sources. In detail, dedicated steps would have to be taken such as (1) characterizing the chamber with respect to its Helmholtz eigenfrequencies, (2) measuring the pressure oscillations frequencies at a location close to the injector, (3) dedicated measurements to capture the phase relationship, (4) measuring the speed of sound for given operating conditions, or, if possible, (5) assessing the combustion chamber temperature and gas properties. At the same time, the objective of the department is its application for wind tunnel experiments, and correspondingly a sufficient characterization, not necessarily doing research on combustion chambers
Fig. 9 assesses the influence of the injectors and the nominal pressure level on the amplitude of the pressure fluctuation. When it comes to the first aspect, i.e. the influence of the injectors, it can be seen that for identical operational settings, the amplitude of the pressure fluctuations can be lowered from > 4 % to < 2 % when using I-1, I-2 or I-3 instead of I-0. Geometrically, this is equivalent to decreasing the annulus region of the injector. The amplitude of the pressure fluctuations also appears to decrease with increasing nominal pressure. However, the latter interpretation is misleading as Fig. 6 shows. Instead, it seems likely that the excitation of the fluctuations is susceptible to a certain pressure level. For the conditions in Fig. 6, it appears to be in the vicinity of 4.5 MPa where the amplitudes grow during ramp up and ramp down. Correspondingly, the amplitude rather depends on proximity of the nominal pressure level to a presumed excitation pressure and how fast this excitation pressure level is passed during ramp up or down. The reason for this presumable sensitivity remains unclear.
The maximum pressure oscillation and the combustion chamber pressure where it occurs was

extracted from Fig. 9 and plotted along with the data from all other operational settings in Fig. 10. Two findings can be drawn here: First, for the given conditions, it shows that injector I-0 is the least favourable design with pressure fluctuations up to > 4 %, while < 2 % can be reached with the other injectors. Having that said, keep in mind that the other injectors have predominantly been tested where I-0 showed relatively strong oscillations, meaning it cannot be excluded that these injectors show a sensitivity to other flow conditions. Second, the size of the nozzle throat diameter has an impact on the oscillation. A smaller throat diameter has a decreasing effect on oscillations (see D_{th} = 8.2 mm vs. 8.0 mm for I-0) for OFR = 5.0, while they are amplified for the lower mixture ratio OFR = 3.3.

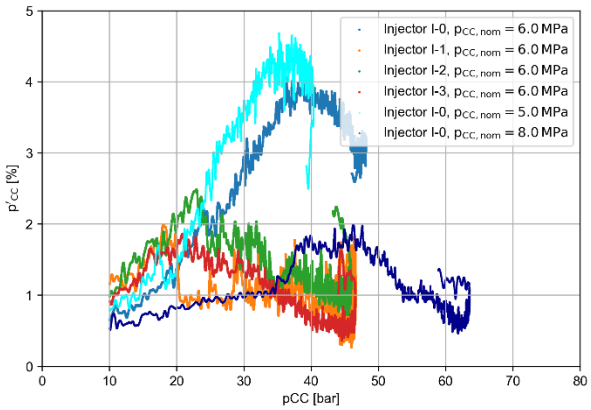

Figure 9. Pressure fluctuation as a function of the chamber pressure for a mixture ratio of OFR = 5.0 (throat diameter D_{th} = 8.2 mm)

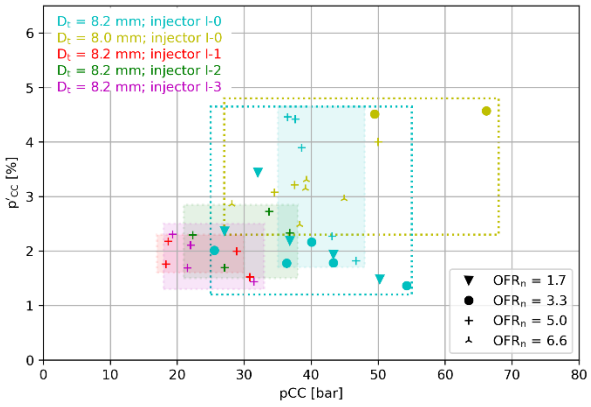

Figure 10. Combustion chamber pressure for the strongest pressure oscillations for all investigated operational settings

As [4] points out, the injector designer should be aware that both low and high frequency instabilities can occur using GH2-GO2 propellants. Further, the authors provide stability criteria for shear mixing elements that provide a guide to stiffness requirements. In their empirical approach, they found that the injector pressure drop can be used as parameter for the stiffness, while it has been found that a pressure drop in the fuel line of $\Delta p_O/p_{CC} > 0.1$ often leads to an unstable configuration with high chamber pressure oscillations.

The graph in literature considering the stability criteria is reproduced in Fig. 11. It depicts the relative pressure drop of the injector for the oxygen and for the hydrogen supply line for the current set of experiments, where mixture ratio, throat diameter and injector geometry can individually be identified. It can be stated that the pressure drops for none of the experiments here is located in the unstable region. This is consistent with the observations regarding the combustion roughness: The observed level for the pressure oscillations was (p'^{p-p}/p_{CC} < 5%), thus the combustion can be described as 'smooth' for all experiments.

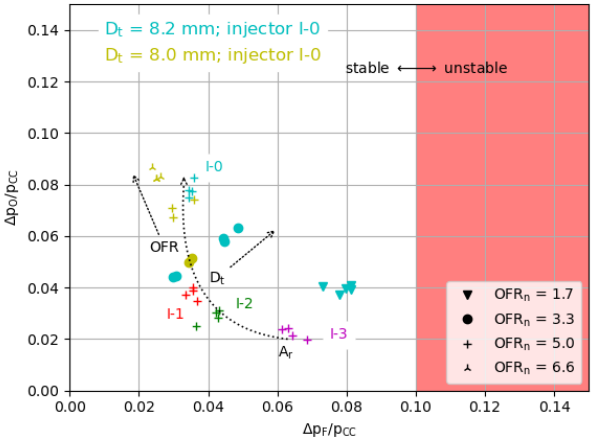

Figure 11. Low frequency stability characteristics of gaseous, shear-mixing injector elements. Representation as given in [4].

Further dependencies are notable in this representation that are useful for the characterization on the one hand, and on the other hand, for the future designs of the injector to avoid hazardous combustion chamber conditions. It can be seen that shifting the mass flow ratios in favour to either of the combustion gases leads to an increased pressure loss in the corresponding supply line as given when adjusting the mixture ratio and the relative area ratio, OFR and A_r, respectively. Increasing the nozzle throat diameter D_{th} leads to an increase of the overall demand of mass flow through the injector. Thus, the pressure losses over both lines increase simultaneously. In other words, a larger throat diameter D_{th} might be unfavourable for the current configuration.

Note that the pressure drop is merely a symptom to assess combustion chamber instabilities, meaning it does not provide direct insights into the spatio-temporal mechanisms that trigger instabilities. Mechanisms such as shear layer or wake instabilities induced by the injector potentially coupling with Helmholtz eigenfrequencies of the combustion chamber. These aspects are better described by assessing the velocity or impulse ratio. Nevertheless, this pressure drop representation is still valuable since it is based on directly and reliably measurable quantities that are linked to ones mentioned before.

To touch the subject of the governing mechanisms possibly feeding the Helmholtz oscillation, the near-

field flow characteristics of coaxial circular jets and the corresponding instabilities are considered as presented in [6]. In comparison to the scenario at hand, this approach based on the
velocity ratio r_u is a first order approximation since it leaves out the combustion and Reynolds number effects. The velocity ratio r_u [20] between the outer and inner velocities denoted as U_o and U_i, respectively, is well suited to describe elements of the overall flow field of coaxial circular jets, and as part of it, the length of the inner potential core region, the mixing characteristics and to assess the instability effects as source for fluctuations.
This description is followed up on by means of the excerpt table Tab. 5 of an overview presented in [6] to categorize mixing effects into various characteristics regions. Regions I to III are not plotted since the outer jet was always faster for the given set of experiments. In Region IV, the velocity difference is very small ($r_u \sim 0$), which is where wake instabilities Wi play a governing role. Departing from there ($r_u \geq 1.1$), wake instabilities continuously weaken and shear layer instabilities S_i become dominant. Region VI, defined by $r_u \geq 2$, denotes the starting point where 'locking' between the inner and outer shear layer with matching vortex generation frequencies can be observed. Characteristic for region VII ($r_u \geq 6$) is that a recirculation region forms upstream from the fully developed zone between the merging point and the end of the inner potential core region [6].
Transferring this categorization to the current application by expressing the velocity ratio r_u in terms of the mixture ratio OFR, specific gas constant ratio R_{H2}/R_{O2} and area ratio A_r of the injector $r_u = R_{H2}/R_{O2}\ 1/A_r\ 1/OFR$, one receives a categorization map as depicted in Fig. 12. It shows that injector I-0 acts in region IV for higher mixture ratios suggesting that the strong oscillations (relatively seen) a fed by wake instabilities. The other injectors operate in the regions where shear layer mixing is dominant, which is favourable for the combustion process. For a wide range of mixture ratios, these injectors operate in region VI, which is characterized by the locking mechanism between the inner and outer jet. This means that the two layers do not develop independently of each other [15], they feature matching vortex generation frequencies, and the core region is shortened. These aspects are interesting since, it suggests that hydrogen will remain as protective sheath to the combustion chamber wall, while increasing the mixing efficiency for combustion. Except for injector I-3, region VII is only entered for low mixing ratios. For the injector design, it could be an interesting region since the flow feature characteristic for it, the recirculation region, could act as a flame holder ensuring the ignition at a fixed location in the combustion chamber. This might explain why injector I-3 feature the lowest fluctuations (see Fig. 10) and the highest heat loads (see Ch. 3.4).

Table 5. Inner mixing layer characteristics for various ranges of velocity ratios. Wake and shear instabilities are denoted by W_i and S_i, respectively. The following abbreviations are used: 'IVJD' and 'IVJM' denote inner mixing layer's velocity jump direction (curved arrows) and magnitude, respectively; 'St' (Strong), 'D' (Dominant), 'We' (Weak), 'Ne' (Negligible); excerpt of the table provided in [5].

Regions (r_u-range)	W_i	S_i	IFJD & IVJM	Governing
Region IV ($0.9 \leq r_u < 1.1$)	St	We	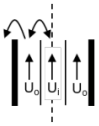 small $\lvert U_o - U_i \rvert$	W_i
Region V ($1.1 \leq r_u < 2$)	We	D	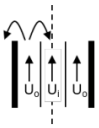 $U_o > U_i$	S_i
Region VI ($2 \leq r_u < 6$)	Ne	D	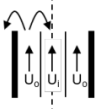 $U_o > U_i$	Locking inner and outer jets
Region VII ($r_u > 6$)	Ne	D	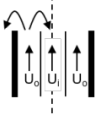 $U_o >> U_i$	Locking inner and outer jets

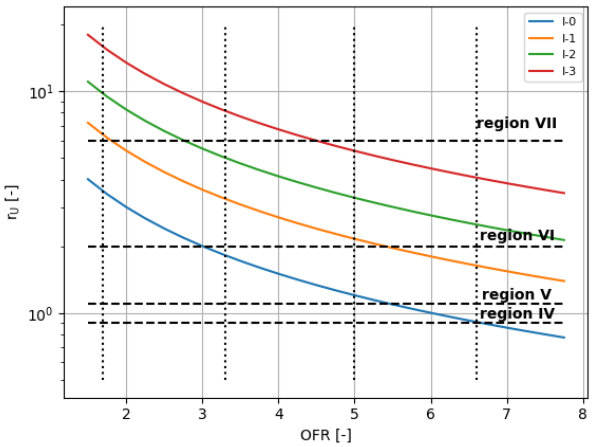

Figure 12. Velocity ratio as function of the mixture ratio and the allocation to characteristic mixing layer regions (see Tab. 5) for the tested injectors

In summary, the findings for this section are as following: Generally, the pressure fluctuations are very small and the combustion is 'smooth' ($p'^{p-p}/p_{CC} < 5\%$). Still smooth combustion, but increased oscillations can be found for injector I-0 ($\sim$ 4% at $p_{CC} \sim 40$ bar), which is the only injector prone to wake instabilities. For the injectors I-1 to I-3, oscillations are small or negligible ($\sim$2%). Overall,

injector I-3 appears to be most promising since, depending on the mixture ration, it might come with a fluidic flame holder. Keep in mind that injector I-3 still has to be tested for other operational settings.
Next, due to the dependency of the oscillations to the injector, or more general to the propellant feed system, and the periodic nature of the oscillation in the low frequency range (200 to 230 Hz), it can be categorized as 'chugging' [25]. To be specific, Helmholtz resonance of the central injector part in the combustion chamber seems to be the governing mechanism for the oscillations. High-frequency oscillations, usually linked to acoustical resonance properties, were not found. For the current setting, the first longitudinal acoustic mode would occur between 2.7 and 3.5 kHz. Last, larger nozzle throat diameters might pose a stability issue according to the empirical finding by [4] (see Fig. 11).

3.4. Temperature and heat flux measurements

Apart from the mechanical loads, the heat load into the combustion chamber is considered to characterize and monitor the operation of the combustion chamber. Thus, thermocouples in the forward and backward cooling supply lines are used for calorimetric measurements. Fig. 13 shows the combustion chamber pressure evolution next to the heat flux evolution into the cooling water for the various injector geometries and various mixture ratios. To eliminate the temporal dependency, the heat flux is additionally plotted versus the chamber pressure.
First, it can be seen that the pressure evolution for the same setting and different injector geometries does not allow for the deduction of a systematic behaviour. The pressure curves coincide with small differences. Next, the plots show that the chamber is in a transient state for all operational settings. Despite the impression that the chamber pressure is levelling out, it can be seen that the heat flux is still increasing. Then, the plots show that with increasing mixture ratio, the heat flux into the cooling water increases as well. Last, it can be seen that for identical input conditions, the heat flux is comparable for all injectors, but for I-3. For injector I-3, the heat flux is substantially increased.
To see it if the latter finding is consistent throughout the experiments, the heat flux into the cooling water at 12 s into the operation is depicted in Fig. 14 for various runs targeting different nominal pressure levels. This graph shows that the increased heat flux of about +25 % for injector I-3 in comparison to the same runs with different injectors remains even surpassing the flux for higher the more demanding mixture ratio of 6.6.
The thermocouples along the inner surface of the combustion chamber are intended to provide further insights into the temperature distribution in the axial direction. Exemplary results are provided in Fig. 15 for the reference configuration (injector I-0, OFR = 5.0, $p_{CC,nom}$ = 8.0 MPa). It can be seen that the temperature increases over time, on the one hand, and on the other hand, the temperature also increases in the downstream direction where it peaks at about 169 mm downstream from the injector plate. However, the curves also reveal large temperature fluctuations of the order of 50 to 100°C (see x = 100 mm or 168.75 mm, respectively). For x = 137.5 mm, temperature jumps in the order of 300°C can be detected.
This is a rather atypical behaviour for temperature measurements and is attributed to the nature of the measurement: the thermocouples are flush-mounted in open tabs along the surface of the inner wall. In other words, the temperature sensitive tip is exposed to the flow field of the combustion chamber and might or might not be in contact with the combustion chamber wall. In other words, it is not clear what exactly is measured except for the temperature at the tip of the sensor. Having that stated, the fluctuations may be a result of unsteady or transient combustion flow effects in the chamber, or vibrations with contact the cold combustion chamber wall.
It seems rather speculative to associate either of the effects to the temperature evolution. If targeted as research questions, dedicated tests are required to deduce the governing mechanisms. Additionally, closed temperature tabs might be favourable to eliminate ambiguities. Nevertheless, it seems reasonable to use that information for qualitative comparisons between runs as done in Fig. 16 for the various injectors in use since the same measurement conditions apply for all runs.

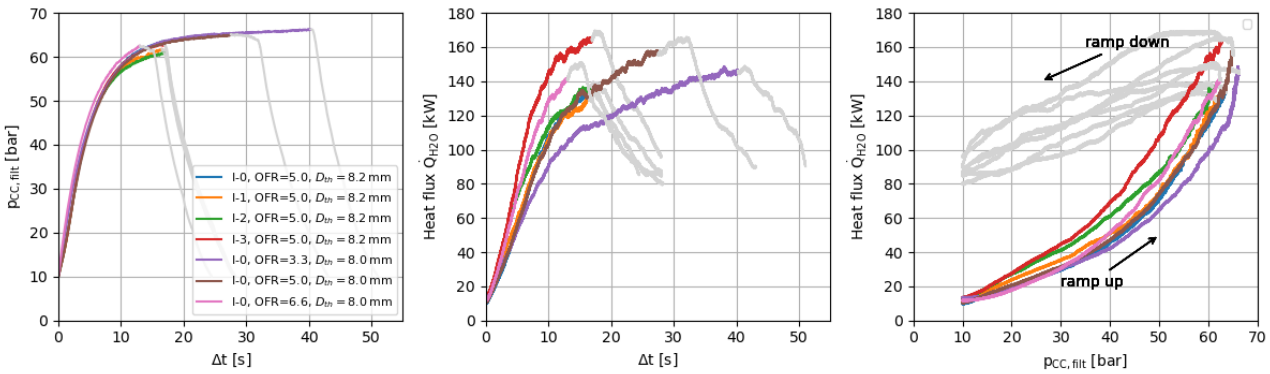

Figure 13. Combustion chamber pressure evolution (left), integral cooling power evolution (mid), and chamber pressure vs. integral cooling power (right).

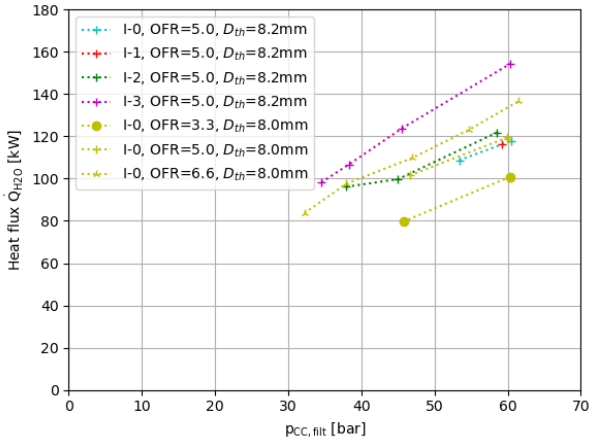

Figure 14. Heat flux into the cooling water 12 seconds into operation

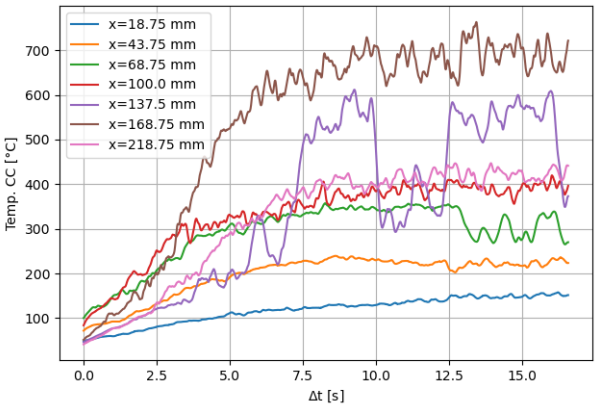

Figure 15. Temporal temperature evolution along the surface of the combustion chamber for the reference run with injector I-0 at a mixture ratio of 5.0 for a nominal pressure of $p_{CC,nom}$ = 8.0 MPa

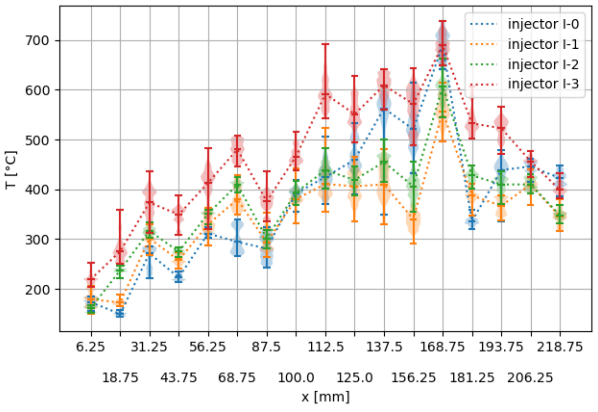

Figure 16. Violine plot of the temperature evolution along the surface of the combustion chamber for the three injectors in use at the operational setting for a mixture ratio of OFR = 5.0, a nominal pressure of $p_{CC,nom}$ = 8.0 MPa, and a throat diameter of D_{th} = 8.2 mm. The last temperature information of the three seconds before the ramp down are used.

For all runs, the temperature increases in the axial direction and reaches a peak at about 169 mm downstream from the injector face. Further, it shows that injector I-3 again measures the highest temperature along the surface of the wall. This observation can be made right from the injector inlet at x = 18.75 mm: Thus, the conditions generated by injector I-2 and I-3 seem to promote a combustion close to the injector face.

Last, the temperature evolution in the combustion chamber wall is discussed by means of Fig. 17. This graph shows the results of four thermocouples placed in the lower or upper third of the combustion chamber (x = 31.25 mm, 43.75 mm or 193.75 mm, respectively) at a radial distance of r = 37.7mm or 56.3 mm from the axial centerline, which corresponds to a depth of r_s = 18.8 mm or 37.3 mm from the surface of the wall. For comparisons between the runs, only the thermocouple (at x = 193.75 mm and r_s = 18.8 mm) that captures the highest heat load is used.

As shown in the temperature distribution in the previous graph (Fig. 16), the heat transfer predominantly takes place in the second and last third of the combustion chamber. This is equally reflected in the temperature evolution of the sensors in the wall: Thus, it seems evident that the sensor closest to the inner wall in the upper third at 193.75 mm downstream from the face plate is most exposed to the heat. At this location, the highest heat loads can be found when using injector I-3, or when operating with the highest mixture ratio at 6.6. For none of the experiments, the temperature exceeds a temperature level, which could critical for the operation of the combustion chamber. Rather the opposite can be stated, meaning the results project confidence in the combustion chamber and suggest that longer run times are feasible. Further, the results can be used as baseline for modelling the heat flow.

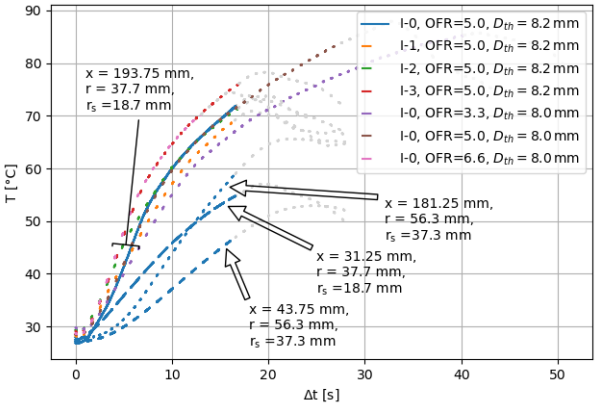

Figure 17. Temperature evolution in the combustion chamber wall for various injectors and mixture ratios.

4. CONCLUSIONS

The objective was to demonstrate and qualify high mixture-high pressure tests in HPTF, and to extend and explore the operational range. This was achieved with the use of the HOC2 combustion chamber. The set-up is now qualified for test from as low as 0.8 MPa up to a combustion chamber

pressure 6.5 MPa between a mixture ratio of OFR = 0.7 and 6.6 for more than 40 s. Longer run times and higher heat load runs are ready to be tested.
Overall, the combustion was found to be smooth with generally weak pressure fluctuations in the range of 2 % oscillating with a distinct frequency at 200 or 230 Hz. The frequency range and the independence to (most) of the flow parameters suggest that the Helmholtz resonance of the central injector part is the driver for these oscillations. The oscillations are influenced by the injector selection. This indicates that the mixing process modifies and feeds the oscillation to a certain degree. In that sense, injector I-3 has shown the most promising results with low to negligible fluctuations. Moreover, this injector also returns the highest heat load indicating an improved mixing process of the combustion gases. Additionally, this injector operates in a region where typically a recirculation region between the inner and the outer jet of the two combustion gases can be found. This leads to a future working hypothesis for the setup at hand with injector I-3 where a recirculation region is acting as a flame holder close to the injector face plate.

5. OUTLOOK

In the future, the current set-up will be used again to extend the operational range of HPTF. Experiments with oxygen-rich combustion are feasible, yet untouched. Further, HPTF is designed to run tests up to 11.5 MPa.
Next, the combustion chamber HOC2 is rather bulky and cannot directly be used for integrated wind tunnel tests. Nevertheless, depending on the scenario, it might make sense to use HOC2 purely as a gas generator from where the hot combustion gases are fed to a wind tunnel model. This can reduce the complexity of wind tunnel model design with an integrated combustion chamber since no requirements are imposed onto the wind tunnel model regarding the mixing length of the combustion gases, required chamber volume, ignition, etc.
Last, currently work is done to extend the capabilities of HPTF to accommodate methane as an additional option for fuel gas. This development is driven due to the shift towards methane-based space launch propulsion systems in the recent years. Consequently, the extension of HPTF's capability will allow i.a. to study exhaust plume effects as induced by retropulsion manoeuvres with the native propellant ensuring the most similar conditions for aerodynamic duplication of the real-flight similarity parameters. A corresponding combustion chamber is under development. All in all, these options will broaden the spectrum of applications for HPTF.

6. REFERENCES

1. Allison, P.M., Driscoll, J.F., Ihme, M. (2013). Acoustic Characterization of a Partially-Premixed Gas Turbine Model Combustor: Syngas and Hydrocarbon Fuel Comparisons. *Proceedings of the Combustion Institute* **34**, 3145–3153.

2. Alster, M. (1972). Improved Calculation of Resonant Frequencies of Helmholtz Resonators. *Journal of Sound and Vibration* **24**, 63–85.

3. Bärow, E. (2018). Untersuchung thermoakustischer Instabilitäten von Sprayflammen. *Forschungsberichte aus dem Institut für Thermische Strömungsmaschinen, Logos Verlag Berlin GmbH*. URL: https://books.google.de/books?id=m7SCDwAAQBAJ.

4. Calhoon, D., Ito, J., Kors, D. (1973). Investigation of Gaseous Propellant Combustion and Associated Injector/Chamber Design Guidelines. *Technical Report NASA-CR-121234, Document ID 19730021067*.

5. Harrje, D.T. (1972). Liquid Propellant Rocket Combustion Instability. *Scientific and Technical Information Office, National Aeronautics and Space*, **194**.

6. van Hout, R., Murugan, S., Mitra, A., Cukurel, B. (2021). Coaxial Circular Jets — A Review. *Fluids* **6**, 147.

7. Kirchheck, D., Gülhan, A. (2016). GH2/GO2 Supply Facility for Hot Plume Testing in the Vertical Test Section Cologne (VMK), in: *Sonderforschungsbereich/Transregio 40 – Annual Report.* URL: https://elib.dlr.de/114008/.

8. Kirchheck, D., Gülhan, A. (2017a). Interaktionsteststand für realistische Raketentreibstrahlen mit umströmender Atmosphäre, in: *Deutscher Luft- und Raumfahrtkongress (DLRK)*, Munich, Germany. URL: https://elib.dlr.de/128664/.

9. Kirchheck, D., Gülhan, A. (2017b). Launch of the GH2/GO2 Supply Facility for Hot Plume Testing at DLR Cologne, in: *Sonderforschungsbereich/Transregio 40 – Annual Report*. URL: https://elib.dlr.de/114009/.

10. Kirchheck, D., Gülhan, A. (2018). Characterization of a GH2/GO2 Combustor for Hot Plume Wind Tunnel Testing, in: *Sonderforschungsbereich/Transregio 40 – Annual Report*. URL: https://elib.dlr.de/128662/.

11. Kirchheck, D., Marwege, A., Klevanski, J., Riehmer, J., Gülhan, A., Karl, S., Gloth, O. (2019a). Validation of Wind Tunnel Test and CFD Techniques for Retro-propulsion (RETPRO): Overview on a Project within the

Future Launchers Preparatory Program (FLPP), in: *International Conference on Flight Vehicles, Aerothermodynamics and Re-entry Missions & Engineering (FAR)*. URL: https://elib.dlr.de/137501/.

12. Kirchheck, D., Saile, D., Gülhan, A. (2019b). Spectral Analysis of Generic Rocket Wake Flows with Cold and Hot Exhaust Jets, in: *Sonderforschungsbereich/Transregio 40 – Annual Report*. URL: https://elib.dlr.de/137429/.

13. Kirchheck, D., Saile, D., Gülhan, A. (2019c). Spectral Analysis of Rocket Wake Flow-Jet Interaction by Means of High-speed Schlieren Imaging, in: *8th European Conference for Aeronautics and Space Sciences (EUCASS)*, 1–4 July, Madrid, Spain. doi:10.13009/EUCASS2019-1057.

14. Kirchheck, D., Saile, D., Gülhan, A. (2021). Rocket Wake Flow Interaction Testing in the Hot Plume Testing Facility (HPTF) Cologne, in: Adams, N.A., Schröder, W., Radespiel, R., Haidn, O.J., Sattelmayer, T., Stemmer, C., Weigand, B. (Eds.), *Future Space-Transport-System Components under High Thermal and Mechanical Loads*. Springer, Cham, pp. 145–162. doi:10.1007/978-3-030-53847-7_9.

15. Ko, N., Kwan, A. (1976). The Initial Region of Subsonic Coaxial Jets. *Journal of Fluid Mechanics* **73**, 305–332.

16. Marshall, W., Pal, S., Woodward, R., Santoro, R. (2005). Benchmark Wall Heat Flux Data for a GO2/GH2 Single Element Combustor, in: *41st AIAA/ASME/SAE/ASEE Joint Propulsion Conference & Exhibit*, p. 3572.

17. Marwege, A., Klevanski, J., Riehmer, J., Kirchheck, D., Karl, S., Bonetti, D., Vos, J., Jevons, M., Krammer, A., Carvalho, J. (2019). Retro Propulsion Assisted Landing Technologies (RETALT): Current Status and Outlook of the EU Funded Project on Reusable Launch Vehicles, in: *Paper presented at the 70th International Astronautical Congress,* 21-25 October 2019, Washington D.C., United States. URL: https://elib.dlr.de/132566/.

18. Pal, S., Marshall, W., Woodward, R., Santoro, R. (2006). Wall Heat Flux Measurements for a Uni-Element GO2/GH2 Shear Coaxial Injector, in: *Third International Workshop on Rocket Combustion Modeling*, pp. 13–15.

19. Ponomarenko, A. (2014). RPA: Tool for Rocket Propulsion Analysis, *Space Propulsion Conference 2014*, Cologne, Germany.

20. Rehab, H., Villermaux, E., Hopfinger, E. (1997). Flow Regimes of Large-Velocity-Ratio Coaxial Jets. *Journal of Fluid Mechanics* **345**, 357–381.

21. Press release (2003). Arianespace Flight 157 - Inquiry Board Submits Findings. https://www.esa.int/Enabling_Support/Space_Transportation/Arianespace_Flight_157_-_Inquiry_Board_submits_findings2. [Online; accessed 06-November-2023].

22. Saile, D., Gülhan, A., Banuti, D., Kitsche, W., Henckels, A., Wyborny, D., Willert, C., Fischer, M., Heinze, J., Voges, M. (2013). Hot Plume Testing Facilities for ELV Propulsion Characterization. *Technical Report*. URL: https://elib.dlr.de/127569/.

23. Saile, D., Kirchheck, D., G ülhan, A., Banuti, D. (2015a). Design of a Hot Plume Interaction Facility at DLR Cologne, in: *8th European Symposium on Aerothermodynamics for Space Vehicles (ATD)*, Lisbon, Portugal. URL: https://elib.dlr.de/99082/.

24. Saile, D., Kirchheck, D., Gülhan, A., Serhan, C., Hannemann, V. (2015b). Design of a GH2/GOX Combustion Chamber for the Hot Plume Interaction Experiments at DLR Cologne, in: *8th European Symposium on Aerothermodynamics for Space Vehicles (ATD)*, Lisbon, Portugal. URL: https://elib.dlr.de/99108/.

25. Sutton, G.P., Biblarz, O. (2001). Rocket Propulsion Elements. Volume 7. *John Wiley & Sons*.

26. Tucker, P., Menon, S., Merkle, C., Oefelein, J., Yang, V. (2008). Validation of High-Fidelity CFD Simulations for Rocket Injector Design, in: *44th AIAA/ASME/SAE/ASEE Joint Propulsion Conference & Exhibit*, p. 5226.

27. VMK. Vertical test section (VMK). https://www.dlr.de/en/research-and-transfer/research-infrastructure/vertical-test-section-vmk. [Online; accessed 07-November-2023].